THE JOURNAL OF PHYSICAL CHEMISTRY B

Article

pubs.acs.org/JPCB

Biamphiphilic Ionic Liquid Induced Folding Alterations in the Structure of Bovine Serum Albumin in Aqueous Medium

Pankaj Bharmoria,[†] K. Srinivasa Rao,[†] Tushar J. Trivedi,[†] and Arvind Kumar*[,†,‡]

[†]Academy of Scientific and Innovative Research (AcSIR) and [‡]Central Salt and Marine Chemicals Research Institute, Council of Scientific & Industrial Research (CSIR), G. B. Marg, Bhavnagar-364002, Gujarat, India

Supporting Information

ABSTRACT: 3-Methyl-1-octylimidazolium dodecylsulfate, [C_8mim][$C_{12}OSO_3$], a vesicle forming biamphiphilic ionic liquid (BAIL) (J. Phys. Chem. B 2012, 116, 14363−14374), has been found to induce significant folding alterations in the structure of bovine serum albumin (BSA) in the aqueous medium at pH 7.0. Such alterations have been investigated in detail using various physicochemical and spectroscopic techniques. Different concentration regimes (monomeric, shared aggregation, and post-vesicular) of [C_8mim][$C_{12}OSO_3$]−BSA interactions have been defined through adsorption and binding isotherms using tensiometry and isothermal titration calorimetry (ITC). Fluorimetry, circular dichroism (CD), and dynamic light scattering (DLS) measurements have shown that [C_8mim][$C_{12}OSO_3$] induces a small unfolding of BSA in the monomeric regime at low concentration (designated as C_f), which is followed by a refolding up to critical aggregation concentration (CAC) (designated as C_1). Above C_1, i.e., in the shared aggregation concentration regime, again a small unfolding of BSA was observed up to critical vesicular concentration (CVC) (designated as C_2). In the vesicular and post-vesicular regimes, the BSA remained stable against folding alterations. The kinetic stability of BSA in the vesicular concentration regimes was studied for a month using turbidimetry. It has been found that [C_8mim][$C_{12}OSO_3$] stabilizes BSA against the aggregation which is the major cause of protein destabilization. The present study gives insights for the design of surface active ILs for protein stabilization as a potential replacement for the mixed micelles of conventional surfactants used in detergent industries for enzyme stabilization and as an artificial chaperone.

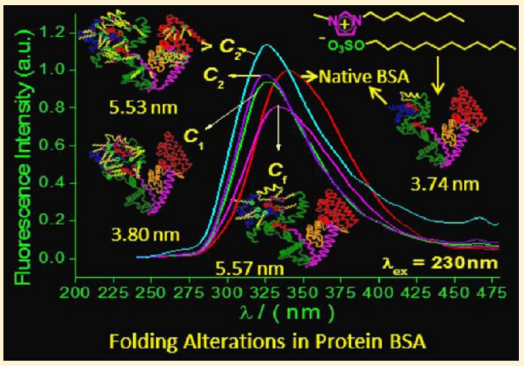

1. INTRODUCTION

Bovine serum albumin (BSA) is a chief transporter of bovine (a mammal) plasma, constituting 3.5−5% of total plasma protein. It is a 66 kDa globular protein having 583 amino acid residues in the single polypeptide chain.[1] Studies on the crystal structure of BSA have revealed that it has a heart shape structure composed of three major domains (I, II, III) which are divided into 9 loops by 17 disulfide bonds. Having binding affinity for an array of compounds such as unesterified fatty acids, bilirubin, bile acids, and many drugs, it acts as a major transporter in the plasma.[2] Its affinity to bind fatty acids has been utilized extensively as a model to study the surfactant−protein interactions,[3−12] attributed to their numerous applications in the field of pharmaceuticals, cosmetics, paints, coatings, detergents, and biochemical reactions.[13−15]

In solution, surfactants (ionic, non-ionic) interact with proteins in various forms such as monomer, shared-micelle, micelle, and vesicle. Applicability of the surfactant−protein formulations depends upon the protein solubilization, its denaturing,[13,14] and renaturing[16,17] on interaction with various forms of surfactant in solution. The binding isotherm of surfactant to protein is mainly divided into three regions, monomeric, sub-micellar, and post-micellar.[5−12] The most studied anionic surfactant sodium dodecylsulfate (SDS) has been reported to stabilize BSA thermally in the monomeric binding region, whereas it denatures the protein in the sub-micellar region.[5,7,8] The recovery of helical content of BSA, denatured in concentrated solution of urea with the addition of a small amount of SDS has also been reported.[16,17] The stabilization effect at low concentration has been attributed to the cross-linking of dodecylsulfate anion between hydrophobic patches of protein and positively charged amino acid residues.[8,18] The cationic surfactants, cetyltriethylammonium chloride (CTAC)[6] and dodecyltriethylammonium bromide (DTAB),[7] and gemini surfactants, 1,2-ethane bis-(dimethyldodecylammonium bromide)[11] and alkanediiyl-α,ω-bis-(dodecyldimethylammonium bromide),[12] have been reported to induce denaturation of BSA even in the monomeric binding regime driven by strong electrostatic interaction with BSA. The effect of ionic surfactants on the conformation of BSA follows the order: cationic > zwitterionic > anionic. These studies have also revealed that, although SDS stabilizes BSA in the monomeric regime compared to cationic and gemini surfactants, all ionic surfactants denature BSA in the sub-

Received: October 15, 2013
Revised: December 19, 2013

   dx.doi.org/10.1021/jp4102042 | J. Phys. Chem. B XXXX, XXX, XXX−XXX

micellar region between the critical aggregation concentration (CAC) and critical micelle concentration (CMC) driven by a cooperative effect of electrostatic and hydrophobic interactions. Using small-angle X-ray scattering (SAXS) and nuclear magnetic resonance (NMR), it has been reported that, in the post-micellar region, BSA forms pearl necklace and bead structures with ionic surfactants where the unfolded protein wraps around the micelle.[10,19]

A report by Lu et al. on the effect of an equimolar mixture of cationic decyltriethylammonium bromide ($C_{10}NE$) and anionic sodium decylsulfonate ($C_{10}SO_3$), surfactants, on the structure of BSA has shown that the mixture did not induce significant changes in the structure of BSA, due to weak interaction indicating the application of mixture as an artificial chaperone.[20] This is due to the fact that the interactions between surfactant ions and BSA are countered by interaction among surfactant head groups. This report inspired us to investigate the effect of a newly synthesized BAIL, $[C_8mim][C_{12}OSO_3]$ (wherein both the cation and anion of ionic liquid are amphiphilic in nature, and works like a catanionic surfactant) on BSA.

Ionic liquids (ILs) (salts having a melting point below 100 °C[21]) are emerging as novel surfactants. Owing to their superior surface activity and tunable property compared to conventional ionic surfactants, surface active ionic liquids (SAILs) have been the topic of significant research interest in the recent years.[22−27] As visionary potential substitutes for conventional ionic surfactants for surfactant−protein applications, SAILs have also been investigated for their interaction and effect on the conformation of proteins. However, such studies have just initiated and only few reports are available in the literature.[28−32] Geng et al. have reported that SAIL, 1-tetradecyl-3-methylimidazolium bromide $[C_{14}mim][Br]$, protects the secondary structure of BSA but destroys the tertiary structure at a low concentration below the CMC.[28,29] Our own group has also reported the effect of SAILs, 3-methyl-1-octylimidazolium chloride $[C_8mim][Cl]$ and 1-butyl-3-methylimidazolium octylsulfate $[C_4mim][C_8OSO_3]$, on protein gelatin and BSA using physical and spectroscopic techniques.[30,31] It was found that $[C_8mim][Cl]$ is more effective in inducing changes in the structure of BSA compared to $[C_4mim][C_8OSO_3]$ at low concentration, whereas both of the ILs denature the protein at higher concentration. Wang et al. have studied the effect of ester-functionalized SAILs, 3-methyl-1-(ethoxycarbonylmethyl)imidazolium dodecylsulfate $[C_1COOC_2C_1im][C_{12}OSO_3]$ and 3-methyl-1-(ethoxycarbonylmethyl)pyrrolidinium dodecylsulfate $[C_1COOC_2C_1Py][C_{12}OSO_3]$, on the stability of BSA and reported that SAIL with a cationic imidazolium headgroup has a higher denaturation effect than that with a pyridinium headgroup.[32]

In the present paper, we have investigated the binding behavior of $[C_8mim][C_{12}OSO_3]$ with protein BSA and alterations induced in the conformation of BSA therein, using various physical and spectroscopic techniques. The used BAIL has been recently reported by us to form vesicles in the aqueous medium.[27] Therefore, various concentration regimes of $[C_8mim][C_{12}OSO_3]$−BSA interactions, viz., pre- and post-vesicular, have been defined by tensiometry and isothermal titration calorimetry (ITC) techniques. The folding alterations in BSA have been investigated using fluorimetry in support with circular dichroism (CD) and dynamic light scattering (DLS) techniques.

2. EXPERIMENTAL SECTION

2.1. Materials. 1-Bromo octane with purity >98% and bovine serum albumin (M.W. = 66463 Da, purity >98.5%) were purchased from SRL, India, and were used as received. 1-Methyl imidazole of AR grade was purchased from Spectrochem, India. Sodium dodecylsulfate (SDS) was purchased from Sigma-Aldrich, Germany. Ethyl acetate and dichloromethane of AR grade were purchased from SD-fine chem. Ltd., India. 3-Methy-1-octylimidazolium dodecylsulfate, $[C_8mim][C_{12}OSO_3]$, was synthesized in our laboratory using the procedure reported elsewhere.[27] The solutions of ILs with or without BSA were prepared weight by volume using an analytical balance with a precision of ±0.0001 g (Denver Instrument APX-200) in phosphate buffer (100 mM, pH 7.0). The buffer solution was prepared in degassed Millipore grade water using AR-grade sodium dihydrogen phosphate and disodium hydrogen phosphate purchased from Merck, India. The concentration of BSA used in the present study is 0.1%. The stock solution of BSA was stored at 4 °C. Scheme 1 depicts the structure of BSA and $[C_8mim][C_{12}OSO_3]$.

Scheme 1. (a) Heart Shape Structure of Bovine Serum Albumin; (b) Chemical Structure of 1-Methy-3-octylimidazolium Dodecylsulfate

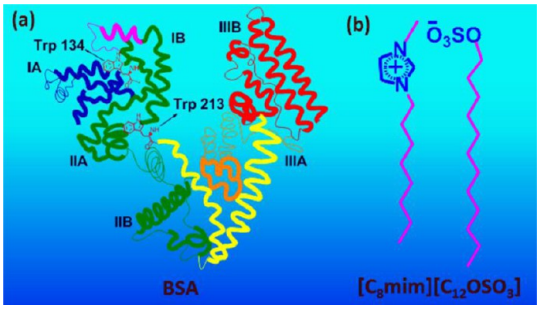

2.2. Methods. *2.2.1. Tensiometry.* Tensiometry has been used to calculate the aggregation concentration of $[C_8mim][C_{12}OSO_3]$ in buffer and to define the concentration regimes of $[C_8mim][C_{12}OSO_3]$ interaction with 0.1% BSA after studying the adsorption isotherms. The technique also gives indirect information about the relative surface excess of surface active species (Γ_{max}) at the interface via the Gibbs adsorption equation (eq 2, Supporting Information). Measurements were carried out at 298.15 K using a Data Physics DCAT II automated tensiometer employing the Wilhelmy plate method. A concentrated solution of $[C_8mim][C_{12}OSO_3]$ (10 times above the aggregation concentration) was added by volume into the base solution, stirred for 3 min, and equilibrated for 5 min before measurement.

2.2.2. Isothermal Titration Calorimetry. Enthalpy changes (dH) due to interaction of $[C_8mim][C_{12}OSO_3]$ with BSA in buffer solution were measured using a MicroCal ITC200 microcalorimeter, with an instrument controlled Hamiltonian syringe having a volume capacity of 40 μL. The titration was done by adding 2 μL aliquots of $[C_8mim][C_{12}OSO_3]$ stock solution into the sample cell containing 200 μL of phosphate buffer or 0.1% BSA solution with continuous stirring (500 rpm). The parameters like time of addition and duration between each addition were controlled by software provided with the instrument. The enthalpy change at each injection was measured and plotted against concentration by using origin

dx.doi.org/10.1021/jp4102042 | J. Phys. Chem. B XXXX, XXX, XXX−XXX

software provided with the instrument. The binding isotherm of $[C_8mim][C_{12}OSO_3]$ binding to BSA was used to define the concentration regimes of $[C_8mim][C_{12}OSO_3]$–BSA interaction.

2.2.3. Fluorimetry. Changes in the tertiary structure of BSA on interaction with $[C_8mim][C_{12}OSO_3]$ were analyzed using a Fluorolog (Horiba Jobin Yvon) spectrometer using a quartz cuvette of path length 1 cm. Changes in the intrinsic fluorescence of BSA were analyzed at an excitation/emission wavelength ($\lambda_{ex}/\lambda_{em}$) of 280/340 nm (slit width = 1 nm) and 230/340 nm (slit width = 5 nm) in a quartz cuvette of 1 cm path length. The maximal values of fluorescence are the average of three measurements. The fluorescence spectra were corrected for the instrumental response.

2.2.4. Far-UV Circular Dichroism Spectroscopy. Secondary structural changes in BSA on interaction with $[C_8mim][C_{12}OSO_3]$ were monitored using a Jasco J-815 CD spectrometer at 298.15 K in the far UV region (λ = 200–250 nm). Spectra were collected in a 1 mm path length quartz cuvette at a scan rate of 50 nm/min and sensitivity of 1000 mdeg. The response time and the bandwidth were 2 s and 0.2 nm, respectively.

2.2.5. Dynamic Light Scattering. Changes in the size of native BSA upon interaction with $[C_8mim][C_{12}OSO_3]$ were monitored at 298.15 K, using a NaBiTec SpectroSize^{300} light scattering apparatus (NaBiTec, Germany) with a He–Ne laser (633 nm, 4 M_w). The hydrodynamic measurements were carried out in a quartz cuvette of 1 cm path length by preparing separate $[C_8mim][C_{12}OSO_3]$–BSA solutions of desired concentrations and measuring their viscosity and refractive indices. The data evaluation of the dynamic light scattering measurements was performed with the inbuilt CONTIN algorithm. The error observed in the size of BSA was ±0.5 nm, and that in the size of vesicle was ±5 nm.

2.2.6. Atomic Force Microscopy (AFM). AFM images of vesicles and BSA–vesicle solution were taken using an Ntegra Aura atomic force microscope (NT-MDT, Russia) in semicontact mode using an NSG-01 silicon probe. Samples were prepared by putting a drop of sample solution on a freshly cut thin mica sheet and dried in air.

2.2.7. Transmission Electron Microscopy (TEM). TEM micrographs of vesicle and BSA–vesicle solution were taken using a JEOL JEM-2100 electron microscope at a working voltage of 80 kV. Samples were prepared by putting a drop of sample solution on the carbon-coated copper grid (300 mesh).

2.2.8. Turbidimetry. Turbidimetry was used to analyze the aggregation of BSA molecules, which is the major cause of protein denaturation. Turbidity of the solution was measured, using a turbidimeter (Eutech TN-100). The sample solutions of BSA in buffer, BSA + 0.44 mM and BSA + 0.8 mM $[C_8mim][C_{12}OSO_3]$, were measured for 1 month at an interval of 3–6 days.

3. RESULTS AND DISCUSSION

3.1. Defining the Concentration Regimes of $[C_8mim][C_{12}OSO_3]$–BSA Interaction. Various concentration regimes of $[C_8mim][C_{12}OSO_3]$–BSA interaction have been defined by studying the adsorption and binding isotherms of $[C_8mim][C_{12}OSO_3]$ in 0.1% BSA solution.

3.1.1. Adsorption Isotherm. Adsorption isotherms of $[C_8mim][C_{12}OSO_3]$ in buffer and in 0.1% BSA solution at 298.15 K are shown in Figure 1. In buffer, the surface tension (γ) decreases steeply before attaining constancy at critical

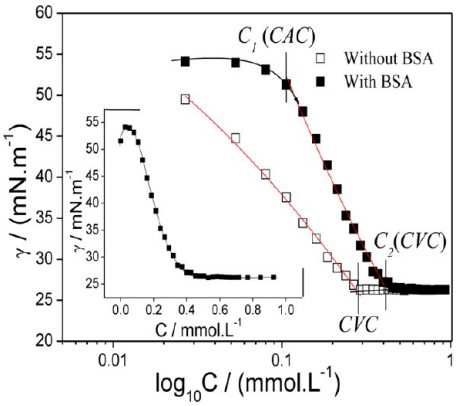

Figure 1. Adsorption isotherms of $[C_8mim][C_{12}OSO_3]$ in buffer and BSA solution. Various transitions discussed in the text are marked with vertical lines. The inset shows the adsorption isotherm of $[C_8mim][C_{12}OSO_3]$ in BSA without a logarithmic scale.

vesicular concentration (CVC), due to the saturation of interface.[33] Compared to $[C_8mim][C_{12}OSO_3]$–buffer system, two definite transitions, critical aggregation concentration, C_1 (CAC), and critical vesicular concentration, C_2 (CVC), have been observed in the $[C_8mim][C_{12}OSO_3]$–BSA system. The inset shows the adsorption isotherm of $[C_8mim][C_{12}OSO_3]$ in 0.1% BSA solution without a logarithmic scale. Initially, there is a small increase in surface tension (γ) at a $[C_8mim][C_{12}OSO_3]$/BSA molecular ratio of 2:1, indicating that initial complexation of $[C_8mim][C_{12}OSO_3]$ to BSA reduces the surface activity of BSA solution. After this small increase, γ remains almost constant up to C_1 ($[C_8mim][C_{12}OSO_3]$/BSA ratio of 7:1), indicating that the $[C_8mim][C_{12}OSO_3]$–BSA (monomer) complexes formed up to this concentration are very less surface active. After C_1, the γ decreases steeply up to C_2 ($[C_8mim][C_{12}OSO_3]$/BSA ratio of 28:1) due to the formation of highly surface active $[C_8mim][C_{12}OSO_3]$/BSA (aggregate) complexes. Above C_2, γ attained constancy because the $[C_8mim]$ and $[C_{12}OSO_3]$ ions have greater interaction (electrostatic and hydrophobic) for each other than to bind with BSA and aggregate freely in the solution to form vesicles after interfacial saturation. The CVC of $[C_8mim][C_{12}OSO_3]$ in 0.1% BSA solution is 0.39 mmol·L^{-1}, which is higher than 0.29 mmol·L^{-1} in buffer solution. The delay of CVC in 0.1% BSA solution indicates the binding of $[C_8mim][C_{12}OSO_3]$ ions to BSA in the solution or at the interface. Various surface parameters such as effectiveness of surface tension reduction (Π_{CVC}), maximum surface excess concentration (Γ_{max}), area of exclusion per monomer (A_{min}), and Gibbs free energy of interfacial adsorption (ΔG°_{ad}) of $[C_8mim][C_{12}OSO_3]$ in buffer and 0.1% BSA solution is calculated using relevant equations (see Annexure 1, Supporting Information) and are given in Table 1. The higher value of Π_{CVC} and high negative value of ΔG°_{ad} for the $[C_8mim][C_{12}OSO_3]$–buffer system indicate that $[C_8mim][C_{12}OSO_3]$ has a higher tendency to reduce the surface tension and has greater feasibility of interfacial adsorption in the absence of BSA. The Γ_{max} is higher and A_{min} is lower for the $[C_8mim][C_{12}OSO_3]$–BSA system, indicating that a maximum amount of surfactant is adsorbed at the interface in the presence of BSA which is due to the interaction of $[C_8mim][C_{12}OSO_3]$ and BSA present at the interface. The feasibility of $[C_8mim][C_{12}OSO_3]$–BSA interaction has been calculated using eq 1.[33]

dx.doi.org/10.1021/jp4102042 | J. Phys. Chem. B XXXX, XXX, XXX–XXX

Table 1. Critical Vesicular Concentration (CVC) from Surface Tension (ST) and Isothermal Titration Calorimetry (ITC)[a]

	CVC (mmol·L^{-1})		parameter			
sample	ST	ITC	Π_{CVC}	$\Gamma_{max} \times 10^6$	A_{min}	ΔG°_{ad}
$[C_8mim][C_{12}OSO_3]$ + buffer	0.29	0.26	35.01	7.19	0.23	−33.80
$[C_8mim][C_{12}OSO_3]$ + 0.1% BSA	0.39	0.42	24.33	11.54	0.14	−30.70

[a]Effectiveness of surface tension reduction (Π_{CVC}), Gibbs' surface excess (Γ_{max}), area of exclusion per monomer (A_{min}), and standard free energy of adsorption (ΔG°_{ad}) at 298.15 K are expressed in mN m^{-1}, mol m^{-2}, nm^2·molecule^{-1}, and kJ·mol^{-1}, respectively.

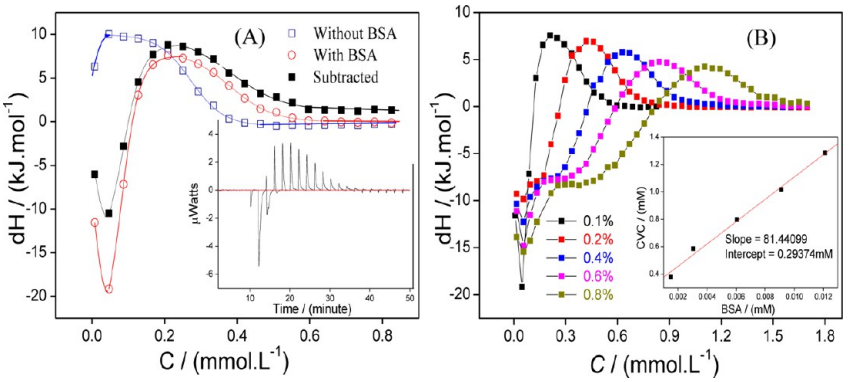

Figure 2. (A) ITC thermograms of $[C_8mim][C_{12}OSO_3]$ aggregation in buffer and binding isotherm with BSA. The inset shows the differential power (dP) plot of $[C_8mim][C_{12}OSO_3]$ binding with BSA at sequential injection. (B) Binding isotherms of $[C_8mim][C_{12}OSO_3]$ binding to BSA at different concentrations of BSA. The inset shows the BSA concentration vs CVC plot of $[C_8mim][C_{12}OSO_3]$.

$$\Delta G^{\circ}_{PS} = \Delta G^{\circ}_{b} - \Delta G^{\circ}_{CVC} = -RT \ln \frac{X_{CAC}}{X_{CVC}} \quad (1)$$

where ΔG°_{PS} is the standard free energy of polymer−surfactant interaction, ΔG°_{b} is the standard free energy of surfactant aggregation on polymer, ΔG°_{CVC} is the standard free energy of aggregation of surfactant in polymer solution, R is the universal gas constant, T is the temperature in kelvin, and X_{CAC} and X_{CVC} are the mole fractions of $[C_8mim][C_{12}OSO_3]$ at the CAC and CVC in 0.1% BSA solution. The calculated value of ΔG°_{PS} = −2.73 kJ·mol^{-1} is very low and indicates that the feasibility of interaction of $[C_8mim][C_{12}OSO_3]$ with BSA is less. This supports the present context of hypothesis that $[C_8mim][C_{12}OSO_3]$ ions have more interaction for each other than for BSA in the solution.

3.1.2. Binding Isotherm. The thermograms of $[C_8mim][C_{12}OSO_3]$ aggregation in buffer and binding isotherm of $[C_8mim][C_{12}OSO_3]$ interaction with BSA at 298.15 K are shown in Figure 2A. The corresponding differential power plot of $[C_8mim][C_{12}OSO_3]$ binding to BSA is shown as an inset in Figure 2A, and that of $[C_8mim][C_{12}OSO_3]$ aggregation in buffer is shown as Figure S1 (Supporting Information). The dilution of $[C_8mim][C_{12}OSO_3]$ in buffer solution is entirely endothermic before aggregation which switches to exothermic in the post-aggregation region. 5.42 kJ·mol^{-1} of dH is absorbed at CVC (0.26 mmol·L^{-1}). To understand the actual enthalpy changes (dH) due to binding of $[C_8mim][C_{12}OSO_3]$ to BSA, the thermogram of $[C_8mim][C_{12}OSO_3]$ aggregation in buffer has been subtracted from that of $[C_8mim][C_{12}OSO_3]$ binding to BSA and is shown in Figure 2A. In the monomeric region, the binding of $[C_8mim][C_{12}OSO_3]$ ion to BSA is entirely exothermic. Initially, there is a strong exothermic increase in dH up to 0.049 mmol·L^{-1} marked as C_f which is due to strong electrostatic interactions of $[C_8mim][C_{12}OSO_3]$ ions with the positive and negative amino acid residue on the protein. The dH at C_f is −10.4 kJ·mol^{-1}. The dH then decreases exothermically with the further addition of $[C_8mim][C_{12}OSO_3]$ and switches to endothermic at a concentration of 0.102 mmol·L^{-1} which is marked as C_1 (CAC). The dH absorbed due to interaction of $[C_8mim][C_{12}OSO_3]$ with BSA at the CAC is 4.46 kJ·mol^{-1}. Above the CAC, dH increases with the further binding of $[C_8mim][C_{12}OSO_3]$ aggregates to BSA via cooperative electrostatic and hydrophobic interaction in the sub-aggregation region, forming $[C_8mim][C_{12}OSO_3]$−BSA (aggregate) complexes. The dH curve then attained a maxima and dH again started to decrease in a sigmoidal manner in the pre-aggregation region before attaining constancy in the post-aggregation region. The dH absorbed due to free aggregation of $[C_8mim][C_{12}OSO_3]$ in solution to form vesicles at the CVC (0.42 mmol·L^{-1}) is 4.46 kJ·mol^{-1}. In the post-aggregation region, the BSA molecules remain either interspersed in between or adsorbed on the vesicle of $[C_8mim][C_{12}OSO_3]$, so no significant change in the dH is observed due to $[C_8mim][C_{12}OSO_3]$ interaction with BSA. To check the binding of an individual ion of $[C_8mim][C_{12}OSO_3]$ to BSA, we have compared our results with the reported binding isotherms of $[C_{14}mim][Br]$−BSA[28] and SDS−BSA[9] systems. Comparing the binding isotherms, it is found that the binding isotherm of the $[C_8mim][C_{12}OSO_3]$−BSA system is more like the SDS−BSA[9] system wherein the interaction of SDS to BSA is exothermic in the monomeric region which switches to endothermic in the aggregation region. The $[C_{14}mim][Br]$ binding to BSA[28] is entirely endothermic. On the basis of this information, we can infer that the initial exothermic enthalpy changes in the $[C_8mim][C_{12}OSO_3]$−BSA system are mainly due to the binding of $[C_{12}OSO_3]$ anion to the cationic sites on BSA via electrostatic interactions. The stoichiometry of $[C_8mim][C_{12}OSO_3]$ ions attached to BSA at the CVC has been quantified by carrying out the isothermal titration of $[C_8mim][C_{12}OSO_3]$ against a varying concentration of BSA (Figure 2B). The number of $[C_8mim][C_{12}OSO_3]$ molecules attached to BSA at the CVC has been calculated from the slope

dx.doi.org/10.1021/jp4102042 | J. Phys. Chem. B XXXX, XXX, XXX−XXX

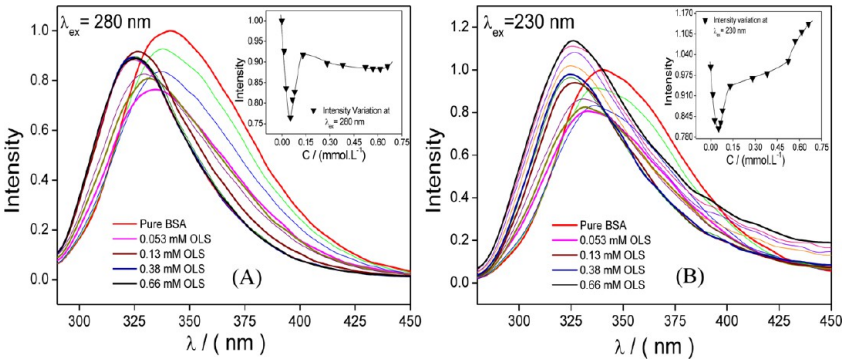

Figure 3. Fluorescence emission spectra of BSA at different $[C_8mim][C_{12}OSO_3]$ concentrations: (A) λ_{ex} = 280 nm; (B) λ_{ex} = 230 nm. The insets show the emission intensity changes of BSA as a function of $[C_8mim][C_{12}OSO_3]$ concentration.

of BSA concentration vs $[C_8mim][C_{12}OSO_3]$ CVC plot using eq 2[34] and is shown as the inset in Figure 2B.

$$[S]_{CVC} = [S]_{Free} + N^*[P] \quad (2)$$

where $[S]_{CVC}$ is the surfactant concentration at CVC, $[S]_{Free}$ is the free surfactant concentration, [P] is the concentration of protein under study, and N is the number of surfactant molecules attached to BSA. From Figure 2B (inset), it is found that 81 molecules of $[C_8mim][C_{12}OSO_3]$ remain attached to the BSA molecule and 0.29 mmol·L^{-1} of surfactant remains free in the solution.

3.2. Folding Alterations in BSA due to $[C_8mim][C_{12}OSO_3]$ Binding. The unfolding−refolding mechanism of BSA due to binding of $[C_8mim][C_{12}OSO_3]$ in the defined concentration regimes has been demonstrated in reference to the alteration in BSA structure at tertiary, secondary level and changes in the hydrodynamic radii, using fluorescence, in support with CD and DLS measurements. A schematic of sequencing of amino acid residues in various domains of BSA is shown in Figure S2 (Supporting Information).[35,36]

3.2.1. Induced Alterations in the Tertiary Structure. Tertiary structural alteration in BSA due to binding of $[C_8mim][C_{12}OSO_3]$ in various concentration regimes has been investigated by observing the changes in intrinsic fluorescence (I_{flr}) of BSA at an excitation (λ_{ex})/emission (λ_{em}) wavelength of 280 or 230 nm/340 nm. BSA absorbs the ultraviolet light at 280 nm due to the n−π^* transition of aromatic amino acid residues and at 230 nm due to π−π^* transition of the protein peptide backbone,[37] as shown in Figure S3 (Supporting Information). Shift in emission wavelength ($\Delta\lambda_{em}$) of protein and variation in I_{flr} are indicative of a change in the microenvironment of the fluorophore and folding alteration in protein. To check the interference of the imidazolium group of $[C_8mim][C_{12}OSO_3]$ during BSA absorption and emission, the UV absorption and fluorescence emission spectra of pure $[C_8mim][C_{12}OSO_3]$ in the concerned concentration regimes of $[C_8mim][C_{12}OSO_3]$ were recorded (Figures S3 and S4, Supporting Information). It is found that compared to BSA the absorption and emission (at λ_{ex} = 280 nm) of $[C_8mim][C_{12}OSO_3]$ are negligible, whereas at λ_{ex} = 230 nm $[C_8mim][C_{12}OSO_3]$ showed only a little emission as compared to native BSA, thus minimizing the contribution of the inner filter effect. The fluorescence emission spectra of the $[C_8mim][C_{12}OSO_3]$−BSA system at λ_{ex} of 280 and 230 nm are shown in Figure 3A and B, and corresponding λ_{em} vs $[C_8mim][C_{12}OSO_3]$ concentration profiles are shown in Figure S5 (Supporting Information).

3.2.1.1. Fluorescence Emission at λ_{ex} of 280 nm. The fluorescence emission spectrum of BSA at λ_{ex} of 280 nm arises due to aromatic amino acid residues like tryptophan (Trp), phenylalanine (Phe), and tyrosine (Tyr). Due to the low quantum yield of Phe, the emission from this residue can be ignored. Therefore, the intrinsic fluorescence of BSA is mainly contributed by Trp and Tyr residues. BSA has 19 tyrosine residues in different domains and two Trp residues (Trp 134 and Trp 213), in domain I and II as intrinsic fluorophores. Trp 134 is present at the protein surface in domain I (subdomain IC), and Trp 213 is present in the hydrophobic binding pocket of protein in domain II (subdomain IIA). At λ_{ex} of 280 nm, the quantum yield of Trp residue has been reported to be more as compared to Tyr residue using synchronous fluorescence spectra.[37] Thus, the quenching or activation of fluorescence in BSA at λ_{ex} of 280 nm will mainly occur if the $[C_8mim][C_{12}OSO_3]$ ion will bind in the vicinity of Trp in domain IC and IIA. Since the CVC of $[C_8mim][C_{12}OSO_3]$ under study is very low and $[C_8mim][C_{12}OSO_3]$ ions have more affinity for self-aggregation, most of the binding of $[C_8mim][C_{12}OSO_3]$ ions to BSA will occur to the charged sites present at the surface of protein.

The I_{flr} of BSA decreases initially up to 0.053 mmol·L^{-1} of $[C_8mim][C_{12}OSO_3]$ (marked as C_f (Figure 3A)) with a slight blue shift due to quenching of fluorescence (Figure S5A, Supporting Information). Trp 134, which is present at the surface of protein in subdomain IC, is surrounded by a number of positively charged lysine and negatively charged aspartic (Asp) and glutamic acid (Glu) residues, which gives the opportunity for both $[C_{12}OSO_3]$ anion and $[C_8mim]$ cation to bind them via electrostatic interactions, causing disturbance in the original conformation of BSA. Above C_f, the I_{flr} started to increase with a blue shift and kept on increasing up to 0.13 mmol·L^{-1} which is just around C_1 (CAC) observed from tensiometric and ITC profiles. Above C_1, the I_{flr} remained almost constant all through the C_2 (CVC) and even at a concentration almost double that of C_2. A blue shift of 16 nm (Figure S5A, Supporting Information) was observed in the I_{flr} up to C_2, which is indicative of conformational alteration in BSA. The increase in I_{flr} above C_f can occur either due to internalization of the fluorophore[31] toward the protein hydrophobic core because of protein refolding where the quantum yield of fluorescence is high or due to increased hydrophobicity around the fluorophore. The latter is feasible if the $[C_8mim][C_{12}OSO_3]$ ion cross-links via electrostatic interactions at one end with the charged amino acid residues and at the other end via hydrophobic interaction with

dx.doi.org/10.1021/jp4102042 | J. Phys. Chem. B XXXX, XXX, XXX−XXX

hydrophobic patches of amino acid residues. BSA has a number of hydrophobic amino acid residues such as leucine (Leu), Tyr, and Phe around Trp 134 in domain IC along with the charged residues which can make this process feasible. The cross-linking effect of $[C_{12}OSO_3]$ anion has been reported earlier by Markus et al. for the stabilization of BSA at very low concentration.[18] In the present case, both statements complement each other. Above C_2, the λ_{em} remained almost constant even at higher concentration, indicating no further changes in the conformation of BSA in the vicinity of fluorophore. This is due to the fact that, above C_2, $[C_8mim][C_{12}OSO_3]$ ion self-interactions predominate over $[C_8mim][C_{12}OSO_3]$–BSA interactions. To check the binding effect of an individual ion of $[C_8mim][C_{12}OSO_3]$ on the conformation of BSA, the fluorescence spectra of BSA with an IL, $[C_8mim][Cl]$, and anionic surfactant, SDS, were recorded in the concerned concentration regime of the $[C_8mim][C_{12}OSO_3]$ and are provided as Figure S6A and B (Supporting Information). The I_{flr} of BSA on interaction with $[C_8mim][Cl]$ decreased continuously, whereas on interaction with SDS it decreased initially up to 0.053 mmol·L^{-1} and then again started to increase before attaining constancy at 0.35 mmol·L^{-1}. Also, there is only a very small blue shift (3 nm) in $[C_8mim][Cl]$–BSA as compared to that observed in SDS–BSA (15 nm) in the studied concentration regime. These results demonstrate that both $[C_8mim]$ and $[C_{12}OSO_3]$ ion of the $[C_8mim][C_{12}OSO_3]$ cause unfolding of BSA but $[C_{12}OSO_3]$ anion is solely responsible for increasing the I_{flr} of BSA. The changes in blue shift also indicate that the $[C_{12}OSO_3]$ anion binds in the vicinity of Trp, thus increasing the hydrophobicity around the fluorophore, whereas the $[C_8mim]$ cation binds in the peripheral sites.

3.2.1.2. Fluorescence Emission at λ_{ex} of 230 nm. The fluorescence emission of BSA at $\lambda_{ex}/\lambda_{em}$ of 230/340 nm has been reported to be the characteristic fluorescence of polypeptide backbone structure[37,38] which can be utilized to understand the conformational alterations in BSA backbone. Although it is reported that at 230 nm electronic absorption arises due to $\pi-\pi^*$ transition in C═O of peptide bond (−HN−CO−),[37] the fluorescence at this λ_{ex} arises from the fluorescent residue (19 Tyr, 2 Trp) present in the peptide backbone where electronic absorption occurs due to $n-\pi^*$ transitions.

Similar to the λ_{ex} of 280 nm, the I_{flr} of BSA decreased, initially up to C_f followed by an increase above C_f (Figure 3B). Contrary to λ_{ex} at 280 nm, here the I_{flr} kept on increasing above C_f at a concentration even much higher that of C_2 (CVC). A blue shift of 15 nm in I_{flr} (Figure S6B, Supporting Information) confirms the conformational alterations in structure of protein due to the change in fluorophore microenvironment. The Stern–Volmer plot at λ_{ex} of 230 nm (Figure 4) at a low concentration of $[C_8mim][C_{12}OSO_3]$ (discussed later) shows the two fluorophore population, thus confirming the alteration in fluorescence due to interaction with both Trp and Tyr residue in BSA backbone. BSA has 12 Tyr residues surrounded by negatively charged and 6 Try residues surrounded by positively charged amino acid residues in different domains, having maximum concentration in domain IC and IIC (Figure S2, Supporting Information). The initial quenching of fluorescence up to C_f arises due to the disturbance of the original conformation of BSA via electrostatic binding of $[C_8mim][C_{12}OSO_3]$ ions at high affinity sites near the fluorophore which also indicates unfolding of protein backbone. The significant increase in fluorescence intensity above C_f can

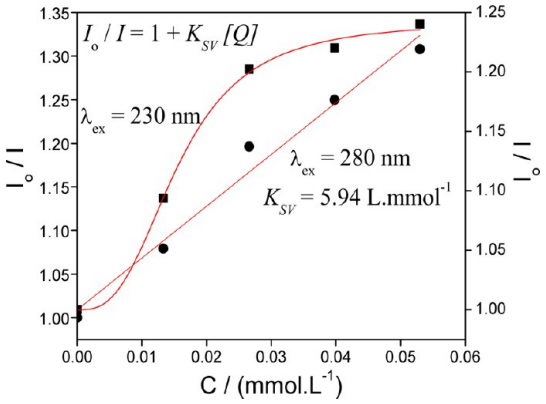

Figure 4. Stern–Volmer plot of the $[C_8mim][C_{12}OSO_3]$–BSA system at λ_{ex} of 230 and 280 nm at low concentration.

occur due to the following reasons: (i) increased hydrophobicity around fluorophore because of protein refolding or $[C_8mim][C_{12}OSO_3]$ aggregation around fluorophore and (ii) $\pi-\pi$ stacking interaction of imidazolium cation with the aromatic ring of the fluorophore residue. The $\pi-\pi$ stacking interaction between the pyridinium ring of surfactant and tryptophan of BSA has been reported earlier by Sun et al. as a reason for increased I_{flr} leading to refolding of protein.[19] This has been confirmed from fluorescence spectra of BSA with an IL, $[C_8mim][Cl]$, and anionic surfactant, SDS (Figure S6C and D, Supporting Information). Contrary to the fluorescence spectra of $[C_8mim][Cl]$–BSA at λ_{ex} of 280 nm (Figure S6A, Supporting Information), the I_{flr} decreased initially, then increased, and then again decreased to reach a minimum at 0.20 mmol·L^{-1}. Above 0.20 mmol·L^{-1}, the fluorescence intensity again increased even beyond that of native BSA (Figure S6C, Supporting Information). A very small blue shift (4 nm) indicates that the significant increase in I_{flr} is principally attributed either to protein backbone refolding or to $\pi-\pi$ stacking interaction of imidazolium cation with the aromatic ring of the fluorophore. In the case of BSA–SDS (Figure S6D, Supporting Information), the I_{flr} decreased initially up to 0.13 mmol·L^{-1} and then started to increase before attaining almost constancy at 0.28 mmol·L^{-1}, with a large blue shift (13 nm). These results show that along with $[C_{12}OSO_3]$ anion the $[C_8mim]$ cation also contributes toward the increase in I_{flr}, indicating possible refolding of protein backbone.

Quenching of the fluorescence can either be dynamic (collision of fluorophore and quencher in the excited state) or static (complex formation between fluorophore and quencher in the ground state). The Stern–Volmer plot can give the idea about quenching efficiency of $[C_8mim][C_{12}OSO_3]$ on binding to BSA in the vicinity of fluorophore and protein backbone. The magnitude of quenching can be interpreted in terms of quenching constant using the Stern–Volmer equation.[31,37]

$$I_0/I = 1 + K_{SV}[Q] = 1 + K_q\tau_0[Q] \quad (3)$$

where I_0 and I are the fluorescence intensity of BSA in the absence and presence of quencher ($[C_8mim][C_{12}OSO_3]$), [Q] is the quencher concentration, and $K_{SV} = K_q\tau_0$ is the Stern–Volmer quenching constant (K_q is the bimolecular quenching constant, and τ_0 is the lifetime of fluorescence in the absence of quencher). In the present system, the quenching of fluorescence occurs only up to a very low concentration both

dx.doi.org/10.1021/jp4102042 | J. Phys. Chem. B XXXX, XXX, XXX–XXX

at λ_{ex} = 280 and 230 nm. Therefore, the Stern−Volmer equation could be plotted only up to 0.053 mmol·L^{-1} and is shown in Figure 4. The Stern−Volmer plot at λ_{ex} = 280 shows quenching of fluorescence with an intercept of 1. The value of quenching constant obtained is 5.94 L·mmol^{-1}. Considering the $\tau_0 = 10^{-8}$ s, the K_q comes out to be 5.94×10^8, which is less than the largest bimolecular quenching constant (2×10^{10}) in aqueous medium, indicating that the quenching of BSA fluorescence by [C_8mim][$C_{12}OSO_3$] is dynamic.[37] The Stern−Volmer plot at λ_{ex} = 230 nm shows quenching of fluorescence in a sigmoidal manner which is a characteristic curve of protein with two kinds of fluorophore populations. This plot indicates that quenching of fluorescence occurs due to binding of [C_8mim][$C_{12}OSO_3$] ions away from fluorophore residues in the protein backbone.

3.2.2. Induced Alterations in the Secondary Structure. Far−UV CD spectroscopy can reveal the alteration induced in the secondary structure (α-helical, β-sheet) of BSA due to unfolding or refolding of protein. As reported by Deep et al.[39] that alterations in the fluorescence intensity cannot solely be considered as a proof of unfolding or refolding of protein, complementary changes in the secondary structure of protein can validate the fluorescence results. The CD spectrum of native BSA and at different concentration of [C_8mim]-[$C_{12}OSO_3$] is shown in Figure 5. The inset in Figure 5

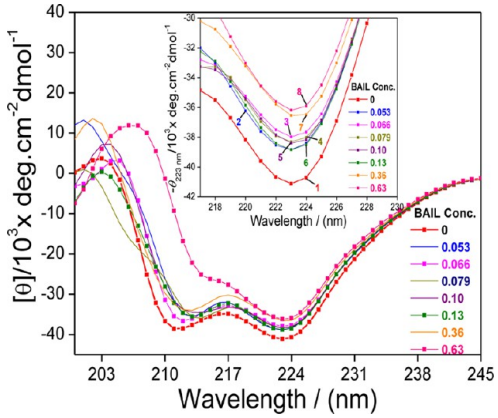

Figure 5. Far-UV CD spectra of BSA as a function of [C_8mim]-[$C_{12}OSO_3$] concentration.The inset shows variation of the $-\theta_{223nm}$ peak.

shows the variation in the $-\theta_{223nm}$ peak at different concentrations of [C_8mim][$C_{12}OSO_3$]. BSA shows two characteristic negative peaks at $-\theta_{212}$ and $-\theta_{223nm}$ due to α-helical structure. The $-\theta_{223nm}$ peak is used to know the qualitative change in α-helical structure,[32] whereas quantitative change in secondary structural (α-helical, β-sheet) content was calculated using K_2D_3 secondary structural analysis software.[40] The $-\theta_{223nm}$ value decreased initially by 7.6% up to 0.066 mmol L^{-1} (C_f), indicating the decrease in α-helical content due to unfolding of protein. Above C_f, the $-\theta_{223nm}$ value increased by 2.27% up to 0.13 mmol·L^{-1} (C_1), indicating the gain in α-helical content due to protein refolding. Above C_1, the $-\theta_{223nm}$ again started to decrease with almost constancy, indicating slight unfolding. There is no change in the wavelength of the $-\theta_{223nm}$ peak which discards the possibility of hydrogen bonding in the system. These results are complementary to the fluorescence results at λ_{ex} of 280 nm and support the fact that increase in fluorescence intensity above C_f is attributed to the refolding of BSA. The quantitatively measured secondary structure variation of BSA as a function of [C_8mim][$C_{12}OSO_3$] concentration is recorded in Table 2 and is shown in Figure S7

Table 2. Variation in the Secondary Structure (α-Helical and β-Sheet) of BSA as a Function of [C_8mim][$C_{12}OSO_3$] Concentration

[C_8mim][$C_{12}OSO_3$] conc. (mmol·L^{-1})	α-helicity (%)	β-sheet (%)
0	68.24	9.32
0.0133	66.30	9.34
0.0265	63.77	9.67
0.0529	62.02	9.86
0.0661	65.25	9.46
0.0792	66.48	9.37
0.1052	66.35	9.42
0.1311	63.25	9.67
0.1824	59.45	10.04
0.258	56.75	10.33
0.3076	62.03	9.79
0.3566	63.24	9.74
0.3809	66.94	9.33
0.5	58.07	10.27
0.638	47.24	12.17
0.727	39.40	13.30

(Supporting Information). BSA in native form exhibits 68.24% α-helical and 9.32% β-sheet structure which is comparable with reported literature values.[41] Quantitatively, it has been observed that BSA undergoes a consecutive unfolding−refolding process. The α-helical content of BSA decreases initially by 9.1% up to C_f followed by an increase of 6.98% up to C_1. Then again, there is a decrease of 14.4% followed by an increase of 17.95% up to C_2. Thus, overall a decrease of 1.94% is observed up to C_2. Above C_2, there is a continuous decrease in α-helical content. Most of the α-helices of BSA are present in subdomains and the section linking different domains. These helices contain numerous positively and negatively charged residues, along with the hydrophobic amino acid residues (Figure S2, Supporting Information). The initial unfolding of BSA up to C_f causes a decrease in α-helical content which opens up the structure of BSA and exposes these helices sequentially. The cross-linking of [C_8mim][$C_{12}OSO_3$] ions with different residues causes refolding of protein with a consequent increase in α-helical content up to C_1. The second decrease in α-helical content can occur due to [C_8mim][$C_{12}OSO_3$] aggregate induced unfolding. This unfolding exposes another helix, which due to cross-linking via [C_8mim][$C_{12}OSO_3$] ions again refolds the protein. This is evidenced by an increase in α-helical content up to C_2. The β-sheet content of BSA varied opposite to the α-helical content in all the concentration regimes (Figure S7B, Supporting Information).

3.2.3. Alterations in the Hydrodynamic Radii. The variation in hydrodynamic radii (R_h) of BSA due to binding of [C_8mim][$C_{12}OSO_3$] has been investigated using DLS measurements. The R_h variation profile of BSA as a function of [C_8mim][$C_{12}OSO_3$] concentration is shown in Figure 6A, and the respective CONTIN plots are shown in Figure S8 (Supporting Information). The R_h of native BSA increased initially from 3.74 to 5.57 nm up to 0.066 mmol·L^{-1} (C_f) due to unfolding of the native structure. Above C_f, the R_h of BSA decreased from 5.57 to 3.82 nm up to 0.10 mmol·L^{-1} (C_1), indicating the refolding of protein. After C_1, the R_h of BSA

dx.doi.org/10.1021/jp4102042 | J. Phys. Chem. B XXXX, XXX, XXX−XXX

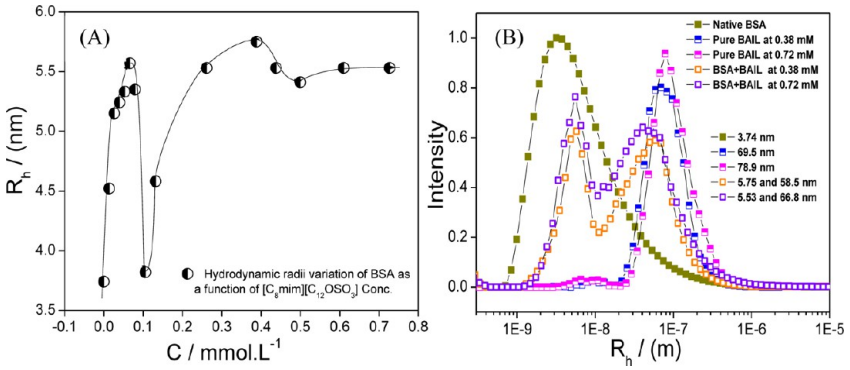

Figure 6. (A) Variation in the hydrodynamic radii (R_h) of BSA as a function of [C_8mim][$C_{12}OSO_3$] concentration. (B) CONTIN plots of native BSA and BSA + [C_8mim][$C_{12}OSO_3$] at different concentrations.

again increased to 5.75 nm up to C_2 either due to protein unfolding or aggregation of [C_8mim][$C_{12}OSO_3$] ions on BSA. Post C_2, the R_h remained constant at 5.53 nm, indicating no more unfolding as the self-aggregation of [C_8mim][$C_{12}OSO_3$] ions predominates over [C_8mim][$C_{12}OSO_3$]−BSA interactions. These results support the postulate that an increase in fluorescence and $-\theta_{223nm}$ above C_f, up to C_1, is due to refolding of BSA. Post CVC, two sizes having R_h 5.53 nm and around 55 nm were observed. The size having $R_h \sim 55$ nm is attributed to the free vesicles of [C_8mim][$C_{12}OSO_3$] in 0.1% BSA solution. Comparative CONTIN plots of vesicle size in buffer and 0.1% BSA are shown in Figure 6B.

The adsorption of BSA on the vesicles was also observed by AFM and TEM micrographs. A comparison of images recorded for pure vesicles and BSA adsorbed vesicles is shown in Figure 7. As expected, there is only a little variation in size of vesicles

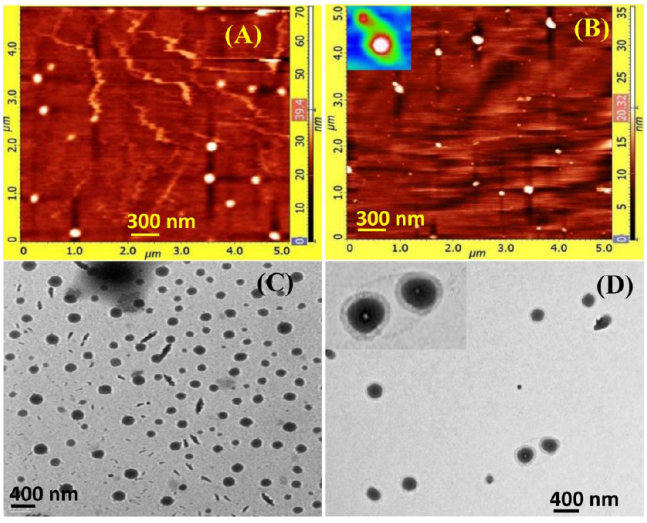

Figure 7. AFM and SEM micrographs of (A and C) [C_8mim]-[$C_{12}OSO_3$] vesicles and (B and D) BSA + vesicles.

upon adsorption of BSA. Scheme 2 depicts the folding alterations in BSA upon interaction with [C_8mim][$C_{12}OSO_3$] in various concentration regimes. Since the size of vesicles is quite larger than BSA, the post-vesicular regime of BSA−[C_8mim][$C_{12}OSO_3$] interaction is separately shown in Scheme 3.

3.3. Kinetic Stability of BSA. Aggregation of protein molecules which is the major cause of protein denaturation has been investigated by turbidity measurements. BSA has 35 cysteine (Cys) residues in its peptide chain, 34 of which form 17 covalent disulfide bonds, resulting in nine loops which act as a bridge between different domains and thus maintain the integrity of protein residue in the most favorable form.[38,39] The 35th Cys residue present in subdomain IA contains a free sulfhydryl group which gives the opportunity to form a covalent sulfide bond between two BSA molecules, leading to aggregation. To check the effect of [C_8mim][$C_{12}OSO_3$] on the BSA aggregation, we measured the turbidity of 0.1% BSA in buffer as well as in post-vesicular regimes (0.44 and 0.8 mmol·L^{-1}) of [C_8mim][$C_{12}OSO_3$] (Figure 8) at different time intervals for 1 month at room temperature. It is found that turbidity of BSA remains almost constant for 13 days in 0.44 mmol·L^{-1} [C_8mim][$C_{12}OSO_3$] and for 18 days in 0.8 mmol·L^{-1} [C_8mim][$C_{12}OSO_3$], indicating the resistance against protein aggregation. It can be possible if the free sulfhydryl group of Cys in subdomain IA is masked, thus preventing the formation of a covalent sulfide bond. The Cys has a number of negatively charged and hydrophobic residues in its vicinity where the [C_8mim] cation can cross-link and thus mask the Cys residue. Inception of aggregation above the listed time can be due to an increase in electrostatic interaction between BSA molecules due to time dependent diffusion in the system. Increased kinetic stability at higher concentration can be attributed to more screening of BSA molecules by increased number of vesicles.

4. CONCLUSION

On the basis of the evidence from fluorescence, CD, and DLS analysis, we conclude that in aqueous phosphate buffer solution (pH 7.0), a biamphiphilic ionic liquid, [C_8mim][$C_{12}OSO_3$], induces significant folding alterations in the structure of protein BSA in different concentration regimes. The [C_8mim]-[$C_{12}OSO_3$] induced small unfolding of BSA in monomeric region (until C_f) due to exothermic electrostatic interactions with the charged amino acid residues present at the surface of protein forming monomer complexes. This has been evidenced by an increase in enthalpy, decrease in I_{flr}, decrease in α-helical content, and increase in R_h. Above C_f, [C_8mim][$C_{12}OSO_3$] induced refolding of protein up to C_1 (CAC) due to cross-linking of BAIL ions via electrostatic interaction at one end and hydrophobic interaction at the other end with the exposed charged and hydrophobic sites of BSA. This has been evidenced by an increase in I_{flr}, an increase in α-helical content, and a decrease in R_h. After C_1, small unfolding of protein was observed up to C_2 (CVC) due to aggregation of [C_8mim]-[$C_{12}OSO_3$] ion at the protein surface via cooperative

dx.doi.org/10.1021/jp4102042 | J. Phys. Chem. B XXXX, XXX, XXX−XXX

Scheme 2. Folding alterations in BSA at variable concentration of $[C_8mim][C_{12}OSO_3]$[a]

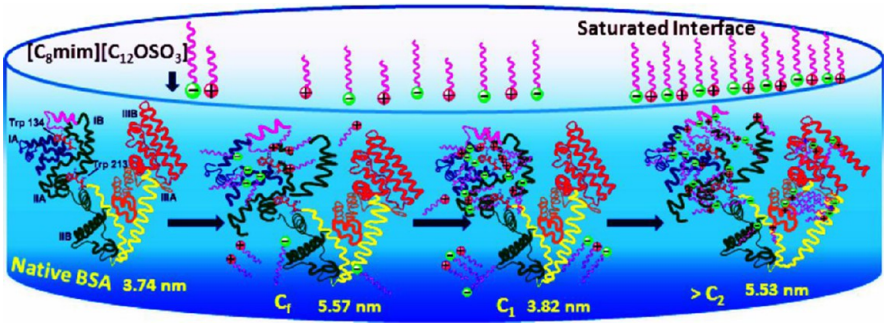

[a] C_f signifies the maximum unfolding concentration due to association of BAIL monomers to BSA; C_1 corresponds to the critical aggregation concentration up to which refolding of BSA occurs due to cross-linking of BAIL ion on BSA, forming BSA−BAIL aggregate complexes; $>C_2$ shows the post-vesicular regime where BSA−BAIL aggregates and BSA adsorbed on vesicles exist.

Scheme 3. The post-vesicular regime where BSA is found interspersed in between and adsorbed on the vesicle

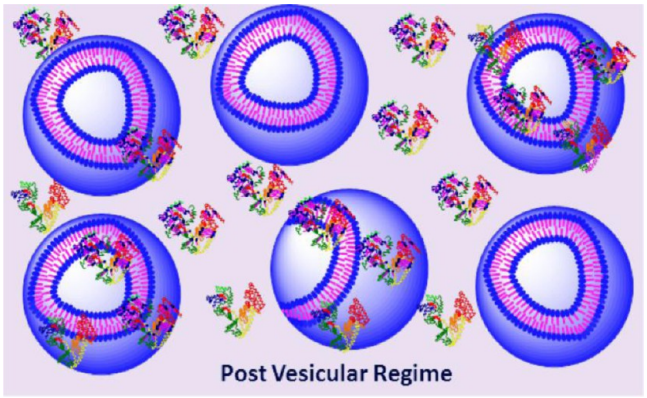

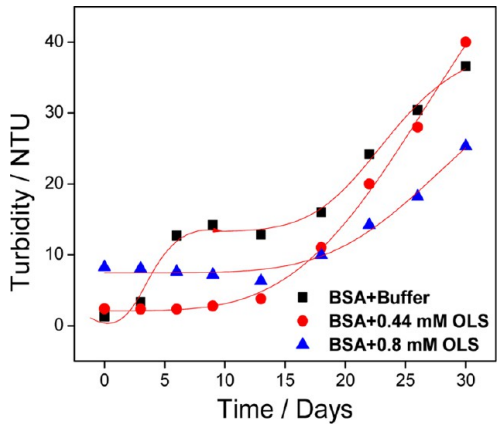

Figure 8. Variation in turbidity of BSA as a function of time in buffer and in $[C_8mim][C_{12}OSO_3]$ at 0.44 and 0.8 mmol·L^{-1}.

electrostatic and hydrophobic interaction. Post C_2 (CVC), no significant folding alterations were observed, as evidenced by negligible variation in I_{flr} (λ_{ex} = 280 nm) and R_h. Due to the strong cooperative hydrophobic and electrostatic interaction between $[C_8mim][C_{12}OSO_3]$ ions, the BAIL ion self-interactions predominate $[C_8mim][C_{12}OSO_3]$−BSA interaction and aggregate in solution at a very low concentration, thus minimizing the effect on protein confirmation as evidenced by low ΔG°_{PS} (−2.73 mmol·L^{-1}) value. In the post-vesicular region, BSA complexed with some ions remains interspersed or attached to vesicles. Evidence from turbidity studies showed that in vesicular solution BSA remained kinetically stable against aggregation and stability increased with the increase in concentration of vesicles. The present study gives vision of using BAILs as a potential substitute for mixed surfactant systems used in protein−surfactant colloidal formulations.[42−44]

■ ASSOCIATED CONTENT

Supporting Information

Calculations for surface pressure, surface excess, area of exclusion per molecule, and free energy of interfacial adsorption. Figures showing a differential power plot, amino acid sequencing, UV spectra, fluorescence spectra, a concentration vs wavelength variation plot, fluorescence emission spectra, quantitative variation of secondary structural content of BSA, and CONTIN plots. This material is available free of charge via the Internet at http://pubs.acs.org.

■ AUTHOR INFORMATION

Corresponding Author

*E-mail: mailme_arvind@yahoo.com; arvind@csmcri.org. Phone: +91-278-2567039. Fax: +91-278-2567562.

Notes

The authors declare no competing financial interest.

■ ACKNOWLEDGMENTS

The authors are thankful to Department of Science and Technology (DST), Government of India, for financial support for this work (No. SR/S/PC-04/2010). The analytical division of CSMCRI is acknowledged for sample characterization. The authors are also thankful to Dr. Tejwant Singh for helpful discussions.

■ REFERENCES

(1) Giancola, C.; Sena, C. D.; Fessas, D.; Graziano, G.; Barone, G. DSC Studies on Bovine Serum Albumin Denaturation. Effects of Ionic Strength and SDS Concentration. *Int. J. Biol. Macromol.* **1997**, *20*, 193−204.

(2) Bujacz, A. Structures of Bovine, Equine and Leporine Serum Albumin. *Acta Crystallogr.* **2012**, *68*, 1278−1289.

(3) Chakraborty, A.; Seth, D.; Setuna, P.; Sarkar, N. Photoinduced Electron Transfer in a Protein-Surfactant Complex: Probing the Interaction of SDS with BSA. *J. Phys. Chem. B* **2006**, *110*, 16607−16617.

(4) Santos, S. F.; Zanetti, D.; Fischer, H.; Itri, R. A Systematic Study of Bovine Serum Albumin and Sodium dodecylsulfate Interactions by

Surface Tension and Small Angle X-ray Scattering. *J. Colloid Interface Sci.* **2003**, *262*, 400−408.
(5) Chen, S. H.; Teixeiria, J. Structure and Fractal Dimension of Protein-Detergent Complexes. *Phys. Rev. Lett.* **1986**, *57*, 2583.
(6) Gelamo, E. L.; Itri, R.; Alonso, A.; da Silva, J. V.; Tabak, M. Small-Angle X-ray Scattering and Electron Paramagnetic Resonance Study of the Interaction of Bovine Serum Albumin with Ionic Surfactants. *J. Colloid Interface Sci.* **2004**, *277*, 471−482.
(7) Kelley, D.; McClements, D. J. Interactions of Bovine Serum Albumin with Ionic Surfactants in Aqueous Solutions. *Food Hydrocolloids* **2003**, *17*, 73−85.
(8) Moriyama, Y.; Kawasaka, Y.; Takeda, K. Protective Effect of Small Amounts of Sodium dodecylsulfate on the Helical Structure of Bovine Serum Albumin in Thermal Denaturation. *J. Colloid Interface Sci.* **2003**, *257*, 41−46.
(9) Chakraborty, T.; Chakraborty, I.; Moulik, S. P.; Ghosh, S. Physicochemical and Conformational Studies on BSA-Surfactant Interaction in Aqueous Medium. *Langmuir* **2009**, *25*, 3062−3074.
(10) Turro, N. J.; Lei, X. G.; Ananthapadmanabhan, K. P.; Aronson, M. Spectroscopic Probe Analysis of Protein-Surfactant Interactions: The BSA/SDS system. *Langmuir* **1995**, *11*, 2525−2533.
(11) Wu, D.; Xu, G.; Sun, Y.; Zhang, H.; Mao, H.; Feng, Y. Interaction Between Protein and Cationic Gemini Surfactant. *Biomacromolecules* **2007**, *8*, 708−712.
(12) Li, Y.; Wang, X.; Wang, Y. Comparative Studies on Interactions of Bovine Serum Albumin with Cationic Gemini and Single Chain Surfactant. *J. Phys. Chem. B* **2006**, *110*, 8499−8505.
(13) Ananthapadmanabhan, K. P. In *Interactions of Surfactants with Polymers and Proteins*; Goddard, E. D., Ananthapadmanabhan, K. P., Eds.; CRC Press, Inc: London, U.K., 1993; Chapter 8. Jones, M. N. *Chem. Soc. Rev.* **1992**, *21*, 127−136.
(14) Jones, M. N. Surfactant Interactions with Biomembranes and Proteins. *Chem. Soc. Rev.* **1992**, *21*, 127−136.
(15) Dalgleish, D. G. In *Emulsions and Emulsion Stability*; Sjoblom, J., Ed.; Marcel Dekker: New York, 1996; Chapter 5.
(16) Moriyama, Y.; Sato, Y.; Takeda, K. Reformation of the Helical Structure of Bovine Serum Albumin by the Addition of Small Amounts of Sodium dodecylsulfate After the Disruption of the Structure by Urea. *J. Colloid Interface Sci.* **1993**, *156*, 420−424.
(17) Moriyama, Y.; Takeda, K. Re-formation of the Helical Structure of Human Serum Albumin by the Addition of Small Amounts of Sodium dodecylsulfate After the Disruption of the Structure by Urea: A Comparison with Bovine Serum Albumin. *Langmuir* **1999**, *15*, 2003−2008.
(18) Markus, G.; Love, R. L.; Wissler, F. C. Mechanism of Protection by Anionic Detergents against Denaturation of Serum Albumin. *J. Biol. Chem.* **1964**, *239*, 3687−3693.
(19) Sun, C.; Yang, J.; Wu, X.; Huang, X.; Wang, F.; Liu, S. Unfolding and Refolding of Bovine Serum Albumin Induced by Cetylpyridinium bromide. *Biophys. J.* **2005**, *88*, 3518−3524.
(20) Lu, R.; Cao, A.; Lai, L.; Zhu, B.; Zhao, G.; Xiao, J. Interaction Between Bovine Serum Albumin and Equimolarly Mixed Cationic−Anionic Surfactants Decyltriethylammonium bromide−Sodium decylsulfonate. *Colloids Surf., B* **2005**, *41*, 139−143.
(21) Rogers, R. D.; Seddon, K. R.; Volkov, S. *Green Industrial Applications of Ionic Liquids*; NATO Science Series; Kluwer: Dordrecht, The Netherlands, 2002.
(22) Bowers, J.; Butts, P.; Martin, J.; Vergara-Gutierrez, C.; Heenan, K. Aggregation Behavior of Aqueous Solution of Ionic Liquids. *Langmuir* **2004**, *20*, 2191−2198.
(23) Wang, H. Y.; Wang, J. J.; Zhang, S. B.; Xuan, X. P. Structural Effects of Anion and Cation on the Aggregation Behavior of Ionic Liquids in Aqueous Solution. *J. Phys. Chem. B* **2008**, *112*, 16682−16689.
(24) Zhao, Y.; Gao, S. J.; Wang, J. J.; Tang, J. M. Aggregation of Ionic Liquids $[C_n\text{mim}][\text{Br}]$ (n = 4, 6, 8, 10, 12) in D_2O: A NMR Study. *J. Phys. Chem. B* **2008**, *112*, 2031−2039.
(25) Singh, T.; Drechsler, M.; Müller, A. H. E.; Mukhopadhyay, I.; Kumar, A. Micellar Transitions in the Aqueous Solutions of a Surfactant-Like Ionic Liquid: 1-Butyl-3-methylimidazolium octylsulfate. *Phys. Chem. Chem. Phys.* **2010**, *12*, 11728−11735.
(26) Rao, K. S.; Singh, T.; Trivedi, T. J.; Kumar, A. Aggregation Behavior of Amino Acid Ionic Liquid Surfactants in Aqueous Media. *J. Phys. Chem. B* **2011**, *115*, 13847−13853.
(27) Rao, K. S.; Trivedi, T. J.; Kumar, A. Aqueous-Biamphiphillic Ionic Liquid Systems: Self-Assembly and Synthesis of Gold Nanocrystal/Nanoplates. *J. Phys. Chem. B* **2012**, *116*, 14363−14374.
(28) Geng, F.; Zheng, L.; Liu, J.; Yu, L.; Tung, C. Interactions between a Surface Active Imidazolium Ionic Liquid and BSA. *Colloid Polym. Sci.* **2009**, *287*, 1253−1259.
(29) Geng, F.; Zheng, L.; Yu, L.; Li, G.; Tung, C. Interaction of Bovine Serum Albumin and Long-Chain Imidazolium Ionic Liquid Measured by Fluorescence Spectra and Surface Tension. *Process Biochem.* **2010**, *45*, 306−311.
(30) Singh, T.; Boral, S.; Bohidar, H. B.; Kumar, A. Interaction of Gelatin with Room Temperature Ionic Liquids: A Detailed Physicochemical Study. *J. Phys. Chem. B* **2010**, *114*, 8441−8448.
(31) Singh, T.; Bharmoria, P.; Morikawa, M.; Kimizuka, N.; Kumar, A. Ionic Liquids Induced Structural Changes of Bovine Serum Albumin in Aqueous Media: A Detailed Physicochemical and Spectroscopic Study. *J. Phys. Chem. B* **2012**, *116*, 11924−11935.
(32) Wang, X.; Liu, J.; Sun, L.; Yu, L.; Jiao, J.; Wang, R. Interaction of Bovine Serum Albumin with Ester-Functionalized Anionic Surface-Active Ionic Liquids in Aqueous Solution: A Detailed Physicochemical and Conformational Study. *J. Phys. Chem. B* **2012**, *116*, 12479−12488.
(33) Tama, K. C.; Wyn-Jones, E. Insights on Polymer Surfactant Complex Structures During the Binding of Surfactants to Polymers as Measured by Equilibrium and Structural Techniques. *Chem. Soc. Rev.* **2006**, *35*, 693−709.
(34) Otzen, D. Protein-Surfactant Interactions: A Tale of Many States. *Biochim. Biophys. Acta* **2011**, *1814*, 560−591.
(35) Brown, J. R. Structure of Bovine Serum Albumin. *Fed. Proc.* **1975**, *34*, 591−591.
(36) Reed, R. G.; Putnam, F. W.; Peters, T., Jr. Sequence of Residues 400−403 of Bovine Serum Albumin. *Biochem. J.* **1980**, *191*, 867−868.
(37) Shu, Y.; Liu, M.; Chen, S.; Chen, X.; Wang, J. New Insight into Molecular Interactions of Imidazolium Ionic Liquids with Bovine Serum Albumin. *J. Phys. Chem. B* **2011**, *115*, 12306−12314.
(38) Sandhya, B.; Hegde, A. H.; Kalanur, S. S.; Katrahalli, U.; Seetharamappa, J. Interaction of Triprolidine Hydrochloride with Serum Albumins: Thermodynamic and Binding Characteristics, and Influence of Site Probes. *J. Pharm. Biomed. Anal.* **2011**, *54*, 1180−1186.
(39) Deep, S.; Ahluwalia, J. C. Interaction of Bovine Serum Albumin with Anionic Surfactant. *Phys. Chem. Chem. Phys.* **2001**, *3*, 4583−4591.
(40) Louis-Jeune, C.; Andrade-Navarro, M. A.; Perez-Iratxeta, C. Prediction of Protein Secondary Structure from Circular Dichroism Using Theoretically Derived Spectra. *Proteins* **2012**, *80*, 374−381.
(41) Mandeville, J. S.; Tajmir-Riahi, H. A. Complexes of Dendrimers with Bovine Serum Albumin. *Biomacromolecules* **2010**, *11*, 465−472.
(42) Bajpai, D.; Tyagi, V. K. Laundry Detergents: an Overview. *J. Oleo Sci.* **2007**, *56*, 327−340.
(43) Sehgal, P.; Mogensen, J. E.; Otzen, D. E. Using Micellar Mole Fractions to Assess Membrane Protein Stability in Mixed Micelles. *Biochim. Biophys. Acta* **2005**, *1716*, 59−68.
(44) Rozema, D.; Gellman, S. H. Artificial Chaperones: Protein Refolding via Sequential Use of Detergent and Cyclodextrin. *J. Am. Chem. Soc.* **1995**, *117*, 2373−2374.